Double-Slit Interference in the Single-Photon Limit

Neil Ghugare

The Ohio State University, Department of Physics, Columbus, OH 43210

April 30, 2026

Abstract

The wave-particle duality of light is a cornerstone of quantum mechanics, describing how light propagates as a delocalized wave yet interacts as a discrete particle. In this experiment, we investigated this phenomenon by performing Young's double-slit experiment in the single-photon limit. Using a laser and a photodiode, we calculate the slit width and slit separation governing our apparatus as 0.084 ± 0.001 mm and 0.411 ± 0.003 mm. Then, using a highly attenuated filament bulb and a photomultiplier tube, we statistically verified that photons traversed the apparatus individually while still building up a classical interference pattern over time. Using the calibrated laser diode geometry, we determined the single-photon source's wavelength to be 561 ± 4 nm. This result is consistent with the accepted value for green visible light, confirming that the interference pattern arises from the self-interference of individual quantum particles, rather than the interaction of multiple photons. This result, however, does disagree with the expected range of our filter of 541-551 nm, which we discuss in detail. We briefly discuss the applications of this result to modern atom interferometry.

1 Introduction

The nature of light has been a subject of debate for centuries. While Isaac Newton originally proposed a corpuscular theory of light, arguing that light's tendency to travel in straight lines and cast sharp shadows necessitated a stream of particles, Thomas Young's double-slit experiment in 1801 provided strong evidence for wave behavior by demonstrating interference, a phenomenon unique to waves [1]. However, Einstein's photoelectric effect later reintroduced the necessity of a particle description, leading to the modern concept of wave-particle duality [1]. In this model, light propagates as a wave but is detected as discrete quanta. The most striking demonstration of this duality occurs when the double-slit experiment is performed with light intensity so low that only one photon traverses the apparatus at a time. The phenomenon of a single, indivisible photon effectively traversing both slits simultaneously to interfere with its own probability amplitude is what Richard Feynman famously called the "central mystery" of quantum mechanics [3]. Under these conditions, the classical wave theory predicts a vanishing interference pattern, while quantum mechanics predicts that individual photons will statistically build up the standard interference pattern over time [3].

Here, we investigate this quantum mechanical limit using an apparatus capable of emitting one photon at a time, justifying this by confirming that the average time between photon emissions significantly exceeds the time of flight through the apparatus. By recording individual photon detection events using a photomultiplier tube (PMT), we statistically verify the single-photon nature of the source and observe the emergence of interference fringes. This experiment confirms that the interference pattern arises not from the interaction of multiple photons, but from the self-interference of single quantum particles. After using a laser to calibrate the apparatus geometry, extracting slit width and slit separation values for our double slit, we can fit our data to a Fraunhofer interference model to extract the wavelength of the incoming light.

While traditionally a proof of quantum mechanics, the 2-slit experiment in the single photon limit motivates modern applications, such as portable atom interferometers, which leverage the wave-particle duality of single atoms to measure gravitational fluctuations with unprecedented precision [7]. By treating a single quantum particle as a delocalized wave that probes multiple paths simultaneously, these sensors enable high-resolution subterranean mapping and GPS-independent navigation, transitioning the double-slit phenomenon from a laboratory demonstration to a critical tool for geophysical and civil engineering [7].

2 Theory

In the classical wave model, light passing through a double-slit aperture produces an intensity pattern resulting from the superposition of the light waves from the two slits. The total intensity is the product of the two-slit interference factor and the single-slit diffraction envelope. For two slits of width a separated by distance b, the intensity $I(\theta)$ as a function of the viewing angle θ is given by the Fraunhofer equation [4]:

$$I(\theta) = I_0 \left(\frac{\sin(\alpha)}{\alpha} \right)^2 \cos^2(\beta), \tag{1}$$

with $\alpha = \frac{\pi a}{\lambda} \sin(\theta)$ and $\beta = \frac{\pi b}{\lambda} \sin(\theta)$, with λ being the wavelength of the light. and I_0 is the maximum intensity at the central peak. For a single slit, the $\cos^2(\beta)$ term vanishes [4].

In our experiment, the detector measures intensity as a function of a linear detector slit position x, not an angle. In the limit where the distance to the detector $D >> x$, we use the small angle approximation $\sin(\theta) \approx (x - x_0)/D$, with x_0 being the center of the diffraction pattern [4], yielding

$$I(x) = I_0 \left(\frac{\sin(A(x - x_0))}{A(x - x_0)} \right)^2 \cos^2(B(x - x_0)), \tag{2}$$

with A and B as fitting parameters related to λ and D (see Appendix B).

3 Experimental Methods

We used the apparatus in Figure 1 to observe the interference in both the high-intensity and single-photon regimes [1]. The setup is contained within a light-tight box to minimize background noise.

To characterize the apparatus' geometry, we first utilized a red diode laser ($\lambda = 0.670 \pm 0.005\ \mu$m) as the light source [1]. The laser provides a coherent, monochromatic beam, producing a well-defined interference pattern, which the photodiode outputs a voltage proportional to this interference intensity [1] (see Appendix A). After aligning the apparatus (see Appendix C), we scanned the detector slit using the micrometer across the pattern to locate the positions of the interference maxima and diffraction minima. We fit this data to Eq. 2 for the near slit, both slits, and the far slit, extracting the slit width a and separation b. These parameters were then held fixed for subsequent single-photon measurements.

For the single-photon experiment, we replaced the laser with a localized filament bulb, which provides incoherent light. To create coherence, the light passes through a single entrance slit before reaching the double-slit, and a green filter is placed in the optical path to isolate a narrow bandwidth of light. The light intensity is measured by the PMT, outputting an amplified voltage of an ejected photoelectron through a photocathode for each individual photon detected [1] (see Appendix A). The PMT is driven by high-voltage supply set to 600V (see Appendix C), with a discriminator threshold set to 0.15V to reject thermal noise while capturing photon events. We justify that this experiment has only one photon in the apparatus at a time in Appendix D.

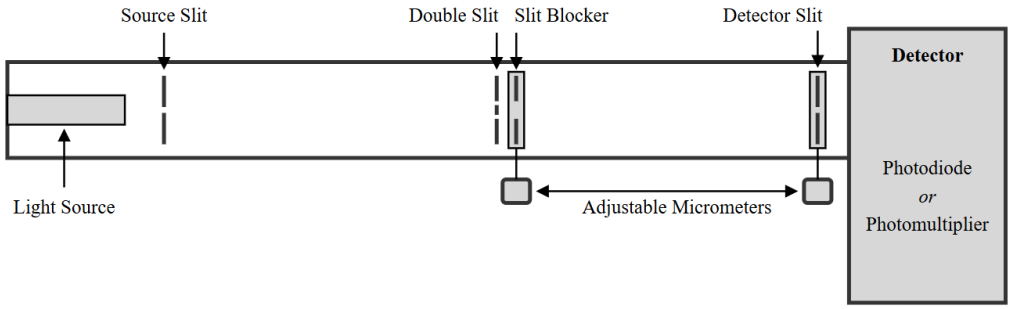

Figure 1: The 2-slit, one photon at a time apparatus. Light passes through the source slit to the double slit and then to the detector [2]. The slit blocker and the detector slit can be moved, driven by micrometers, allowing for selective scanning of different slit configurations and detector slit positions [2]. Two detector options are available, the photodiode or the PMT [2].

4 Data Analysis and Results

To determine the precise geometry of the slit apparatus, we first analyzed the high-intensity diffraction patterns produced by the calibration laser. We fit Eq. 2 to the measured intensity distributions for the near slit, far slit, and double slit configurations (see Appendix B, Figures B.1 and B.2). By

using an Orthogonal Distance Regression (ODR) fit, we extracted the slit width 0.084 ± 0.001 mm and the slit separation 0.411 ± 0.003 mm. The primary sources of uncertainty from this calibration arose from fixed errors in our measurement and micrometer backlash, and systematic uncertainties of the multimeter itself, which were propagated via Eqs. B.7 and B.8.

With the geometric parameters a and b taken from the laser fit, we evaluated the single-photon data collected by the PMT. We fit the discrete photon count distributions to the same Fraunhofer interference model (Eq. 2) to extract the central wavelength of the source filament bulb. The fit yielded a wavelength 561 ± 4 nm. This fitted wavelength falls appropriately within the expected transmission band of the green optical filter [8]. This wavelength, however, does not match the expected wavelength of the green filter of 541-551 nm [1]. The cause of this disagreement is likely due to the blackbody spectrum of the filament bulb causing more longer wavelength photons to be emitted, or due to green filter leakage at the red tail, causing near-IR and deep red photons to pass through the filter, causing a greater average wavelength calculation.

We receive interference patterns as in Figure 2 and those in Appendix B.

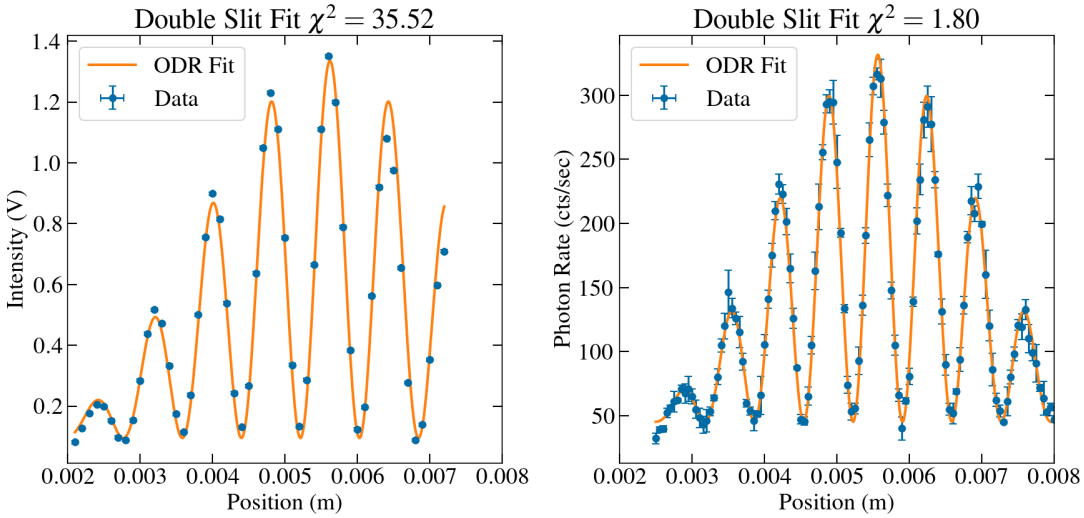

Figure 2: Double slit interference patterns for the laser (left panel) and bulb (right panel). The laser panel has intensity errors due to uncertainties in the multimeter itself and uncertainties in measurement due to varying voltage readings. The error bars are too small to be visible. The reduced χ^2 was calculated to be 35.52, indicating a poor fit, which is due to the asymmetry of the alignment, causing asymmetrical interference patterns, not accounted for in our fit, as seen in the shoulder plot of Figure C.1. The bulb panel has intensity errors from the standard deviation of multiple measurements at each position. The reduced χ^2 here was 1.80, indicating a good fit of the data. Both panels have a fixed position error of $\sigma_x = 0.002$ mm to account for micrometer backlash. For more information on the fitting procedure and extracting fundamental results from these panels and other fits, see Appendix B.

5 Discussion and Conclusions

In this experiment, we successfully observed the emergence of a double-slit interference pattern in the single-photon limit. By first calibrating the apparatus with a classical laser to find the slit dimensions ($a = 0.084 \pm 0.001$ mm and $b = 0.411 \pm 0.003$ mm), we were able to fit the PMT single-photon count data to the Fraunhofer interference model. The extracted wavelength 561 ± 4 nm closely matches the accepted range of the green light, but disagrees with the quoted green filter value, likely caused by blackbody attenuation or filter leakage. These results fulfill our primary goal of demonstrating that individual quanta of light undergo self-interference, completely replicating the classical wave distribution over time. The primary inherent difficulty in our measurement stemmed from the finite detector slit width, which averages the intensity over that width, blurring the sharp interference fringes. We could thus improve the spatial resolution of the interference fringes by utilizing a narrower detector slit. However, this would proportionally decrease the photon transmission rate, necessitating a significantly longer data collection time to overcome the statistical Poisson noise of the dark counts.

Ultimately, the successful observation of single-photon interference in this apparatus directly validates the principles of wave-particle duality that underpin modern quantum sensing [7]. Just as this experiment demonstrates the ability of a single quantum entity to simultaneously probe multiple paths, scaling these foundational mechanics to massive particles enables the unprecedented gravimetric precision of emerging technologies like portable atom interferometers [7]. By verifying these fundamental quantum behaviors in a controlled laboratory setting, we establish the conceptual framework required to translate wave-particle duality into critical tools for subterranean mapping and advanced navigation [7].

References

[1] Two-Slit Interference, One Photon at a Time Operating Manual (Condensed), TeachSpin Inc., (2006).

[2] 2-Slit Interference, 1 Photon at a Time v2.3, Carmen/Canvas, (2022).

[3] Feynman, R., Leighton, R., and Sands, M. The Feynman Lectures on Physics, Vol. 3 (Addison-Wesley, Reading, MA, 1965), Chap. 1.

[4] Two Slit Interference, One Photon at a Time – Pre-Lab Problems, Carmen/Canvas, (2026).

[5] B&K Precision Corp., 4 1/2 Digit and 50,000 Count Bench Multimeters USER MANUAL, (2010). https://assets.testequity.com/te1/Documents/pdf/bk/2831E-5491B_manual.pdf.

[6] Hamamatsu Photonics K.K. Photomultiplier tubes: Basics and applications (3rd ed., Edition 3a) (2007).

[7] Vovrosh, J., Dragomir, A., Stray, B., and Boddice, D. Advances in Portable Atom Interferometry-Based Gravity Sensing, Sensors 23, 7651 (2023).

[8] Bruno, Thomas J. CRC handbook of fundamental spectroscopic correlation charts. Boca Raton, FL: CRC Press, (2006). ISBN 9780849332500.

Supplementary Information

A Detector Functionality

We have two detectors we use in this experiment. One is the photodiode, used for the laser portion of the experiment, and the other is the photomultiplier tube (PMT), used for singular photon events [1]. The PMT has a shutter to protect it from damage, due to its sensitivity to light sources like ambient or room lighting [1]. When using the photodiode, the PMT shutter will always be closed or "down" [1]. We use two detectors since the PMT is incredibly sensitive to large amounts and large intensities of light [1]. The ambient lighting or the laser could damage or destroy the PMT [1]. The photodiode cannot be used for the single photon experiment because its analog current output lacks the sensitivity and internal amplification required to resolve the infinitesimal energy deposits of individual photons against the detector's inherent thermal noise floor.

A.1 The Photodiode

The photodiode is used with the laser light source. With the shutter "down", a 1 cm^2 solid-state photodiode is positioned as the detector, which generates electric current when illuminated [1]. Because the photodiode's 1 cm^2 surface area is large enough to integrate over the entire interference pattern simultaneously, it is masked by a detector slit with an effective width of 0.085 mm [1]. This narrow slit provides the necessary spatial resolution to scan across and measure the intensity profile of the fringes [1]. The photodiode turns the illuminated surface into an electric current able to be measured by a multimeter [1]. This electric current is proportional to the intensity of the laser light, and can be measured at a 2-20V sensitivity [1]. This represents the classical view of light as a continuous field.

A.2 The PMT

The PMT detects single photon events by ejecting a photoelectron from a photocathode [1]. These photoelectrons are then amplified by a factor of about 10^5 inside the PMT, and arrive as a pulse of about 10^5 electrons at the input of the amplifier [1]. The amplifier converts that pulse of negative charges from the electrons into a positive, measurable voltage pulse, which is the output seen at the oscilloscope [1]. It's important to note that the PMT outputs discrete, distinct pulses while the photodiode outputs a continuous voltage [1].

The PMT functions via the photoelectric effect, Einstein's theory that light comes in discrete quanta called "packets" [1]. In particular, the PMT relies on the photoelectric effect when a photon strikes the photocathode to eject an electron, relating to the work function required to eject an electron. When photons strike the photocathode within the PMT, electrons in the photocathode absorb the

photon energy given by the frequency ν via $E = h\nu$ [6]. This causes the electrons to become excited, diffusing toward the surface of the photocathode [6]. If these electrons have enough energy to overcome the vacuum level barrier (also called the work function Ψ), they are emitted into the vacuum as photoelectrons [6]. If the photon energy is lower than the work function, no photoelectrons are emitted [6].

This phenomenon cannot be explained by a classical wave model. In classical electromagnetism, the energy of a light wave is distributed continuously across its wavefront and depends entirely on its intensity (amplitude), not its frequency. Therefore, classical theory predicts that a very bright, low-frequency light should eject electrons, and that at very low intensities, there should be a measurable time delay as the electron "accumulates" enough continuous wave energy to overcome the work function. However, experiments demonstrate that electron emission is completely instantaneous and only occurs if the incident light exceeds a specific threshold frequency, regardless of intensity. This can only be explained by the particle model: light energy is delivered in discrete, localized packets (photons) [3]. A single electron absorbs a single photon, and if that individual photon's energy ($E = h\nu$) is strictly less than the work function (Ψ), no emission can occur [3].

B Approximating and Fitting the Fraunhofer Equations

From earlier, we know that the Fraunhofer equation for a double slit is given by [4]

$$I(\theta) = I_0 \left(\frac{\sin(\alpha)}{\alpha} \right)^2 \cos^2(\beta), \tag{B.1}$$

with $\alpha = \frac{\pi a}{\lambda} \sin(\theta)$ and $\beta = \frac{\pi b}{\lambda} \sin(\theta)$, with λ being the wavelength of the light. and I_0 is the maximum intensity at the central peak. For a single slit, the $\cos^2(\beta)$ term vanishes [4]. Another important note is that the I_0 is not exactly the same for the single slit versus double slit cases. We can fit it just as I_0, but the double slit version should have a relative intensity four times greater than a single slit [4].

For small oscillations, which we can assume since the distance to detector D is much larger than the x distance of the detector slit we use to scan the interference pattern, we can say that $\sin(\theta) \approx \frac{(x-x_0)}{D}$, with x_0 being the center of the interference pattern. Thus, we can see that

$$\alpha \approx \frac{\pi a}{\lambda} \frac{x - x_0}{D}, \tag{B.2}$$

and

$$\beta \approx \frac{\pi b}{\lambda} \frac{x - x_0}{D}. \tag{B.3}$$

However, when fitting the Fraunhofer equations, it is better to encapsulate all the constants into a singular fitting parameter. Thus, we define fitting parameters A and B as

$$A \equiv \frac{\pi a}{\lambda D}, \tag{B.4}$$

and

$$B \equiv \frac{\pi b}{\lambda D}. \tag{B.5}$$

Thus, utilizing the Fraunhofer equation, the small angle approximation, and our fitting parameters, we will fit the following equation:

$$I(x) = I_0 \left(\frac{\sin(A(x - x_0))}{A(x - x_0)} \right)^2 \cos^2(B(x - x_0)). \tag{B.6}$$

Hence, we can then find the slit width a and separation b from the fitted A and B values. We need to make sure to propagate the errors, via

$$\sigma_a = a \sqrt{\left(\frac{\sigma_A}{A} \right)^2 + \left(\frac{\sigma_\lambda}{\lambda} \right)^2 + \left(\frac{\sigma_D}{D} \right)^2}, \tag{B.7}$$

and

$$\sigma_b = b\sqrt{\left(\frac{\sigma_B}{B}\right)^2 + \left(\frac{\sigma_\lambda}{\lambda}\right)^2 + \left(\frac{\sigma_D}{D}\right)^2}, \tag{B.8}$$

where σ_A and σ_B will be given by the fit on the data, and σ_λ will be given from the nominally quoted measurement of the laser. We found that σ_D is negligible compared to the other errors.

We fit the laser data to extract the slit width and slit separation. The fits are given in Figures B.1 and B.2.

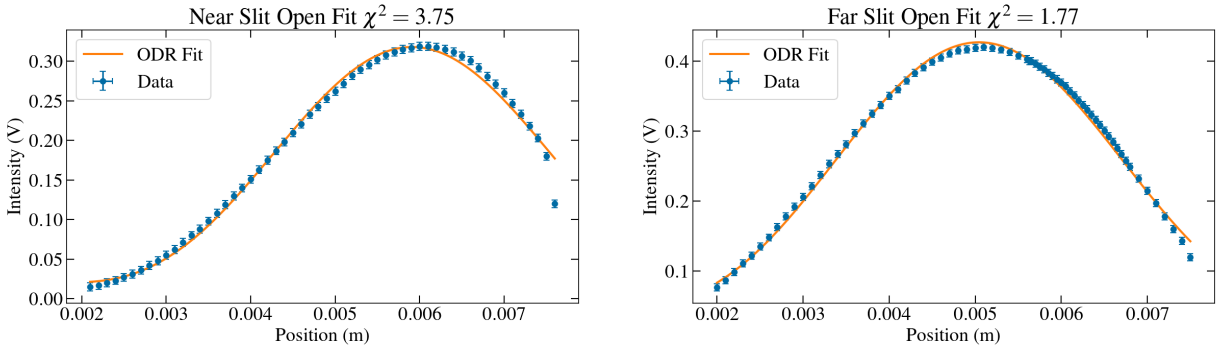

(a) Fit of the Fraunhofer equations to the near single slit.

(b) Fit of the Fraunhofer equations to the far single slit.

Figure B.1: The following figures show the ODR fits (Eq. B.6) for the two single slits in our apparatus, the near slit and the far slit. The reduced χ^2 for the fits are 3.75 and 1.77, respectively, indicating a good fit to the data, with variations occurring from noise or other sources of error. The error bars used for the fit included an error in the position to account for micrometer inaccuracy, given by $\sigma_x = 0.002$ mm. The errors in the intensity were errors from the measurement and the error in the multimeter, added in quadrature. The error in the measurement was $\sigma_V = 5$ mV and the multimeter error given in Table B.1 and Eq. B.9. Using Eq. B.4, we can rearrange and solve for the slit width a and propagate errors using Eq. B.7. This yields slit width values of 0.083 ± 0.002 mm and 0.085 ± 0.002 mm. This provides good agreement with the nominal value of the slit width, quoted at 0.085 mm [1], within a 1σ agreement. For usage with the PMT, we combine both results with a weighted mean and uncertainty (Eq. B.10), yielding an official slit width value of 0.084 ± 0.001 mm.

The error in our BK Precision 2831E multimeter is given by [5]:

$$\sigma_{\text{mult}} = \pm(\%\text{ of reading } + \%\text{ of range }). \tag{B.9}$$

For information on these percentages, see Table B.1.

Range	Resolution	Full Scale	1-Year Accuracy
200.00 mV	10 μV	210.00	0.03% + 0.08%
2.0000 V	100 μV	2.1000	0.03% + 0.05%

Table B.1: BK Precision 2831E multimeter errors for a given range and resolution. The first percentage in the "1-Year Accuracy" column gives the percentage of the read value, while the second percentage acts on the "Range" column [5]. We adopted the manufacturer's 1-year accuracy specifications to provide a conservative estimate of instrumental uncertainty [5].

To combine the values of the slit width, we use a weighted average formula,

$$a = \frac{\frac{a_1}{\sigma_1^2} + \frac{a_2}{\sigma_2^2}}{\frac{1}{\sigma_1^2} + \frac{1}{\sigma_2^2}} \text{ and } \sigma_a = \sqrt{\frac{1}{\frac{1}{\sigma_1^2} + \frac{1}{\sigma_2^2}}}. \tag{B.10}$$

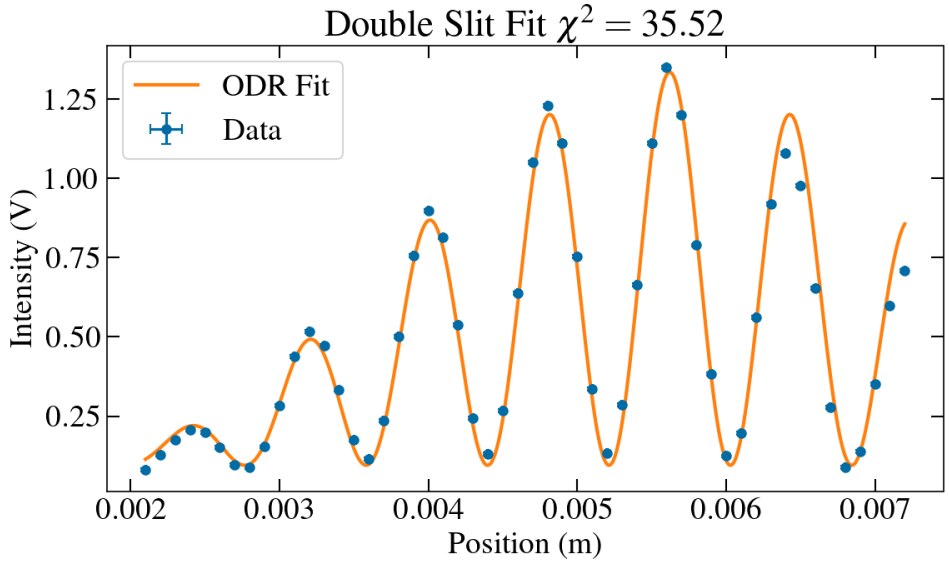

Figure B.2: This figure shows the ODR fit for the double slit (Eq. B.6). We use the same errors in the position $\sigma_x = 0.002$ mm and errors in the measured voltage as $\sigma_V = 5$ mV with errors from the multimeter added in quadrature via Eq. A.9 and Table B.1. The error bars here are too small to be visible. The fit yields a reduced χ^2 of 35.52, which indicates a poor fit. We explain this discrepancy by the asymmetry in the experimental data, which is not accounted for in the Fraunhofer fit function we used. This asymmetry is due to imperfect alignment, as seen in the shoulder plot in Figure C.1. When fitting, we extract the slit separation value b as 0.411 ± 0.003 mm, using Eqs. B.5 and B.8. Compared to the nominal value of 0.406 mm [1], we see agreement to 1.67σ.

For the PMT, we will be fitting the same equation (Eq. B.6), but we will use or calculated a and b values, and calculate the unknown wavelength λ (Young's calculation). As such, we will be

calculating

$$\lambda = \frac{\pi a}{AD} \tag{B.11}$$

for a single slit, and we'll also calculate

$$\lambda = \frac{\pi b}{BD} \tag{B.12}$$

for the double slit, expecting good agreement. The errors, then, will be propagated via

$$\sigma_{\lambda,A} = \lambda \sqrt{\left(\frac{\sigma_a}{a}\right)^2 + \left(\frac{\sigma_A}{A}\right)^2 + \left(\frac{\sigma_D}{D}\right)^2} \tag{B.13}$$

and

$$\sigma_{\lambda,B} = \lambda \sqrt{\left(\frac{\sigma_b}{b}\right)^2 + \left(\frac{\sigma_B}{B}\right)^2 + \left(\frac{\sigma_D}{D}\right)^2}. \tag{B.14}$$

Once again, we will ignore the σ_D term, as it is negligible compared to the other errors.

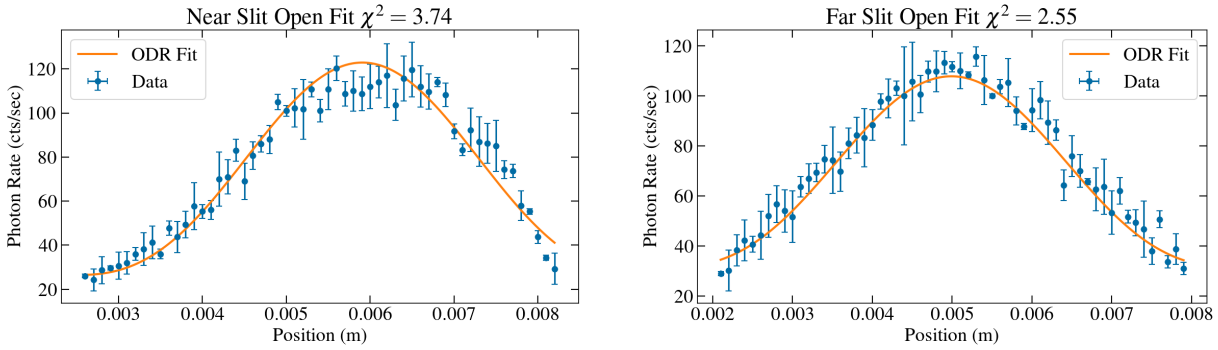

(a) PMT fit of the Fraunhofer equations to the near slit.

(b) PMT fit of the Fraunhofer equations to the far slit.

Figure B.3: The following figures show the ODR fits (Eq. B.6) for two single slits in the PMT experiment. The reduced χ^2 for these fits are 3.74 and 2.55, respectively, indicating a good fit to the data, with variations occurring from noise, variations in the data collection, and other sources of error. The error bars used for the fit include an error in the micrometer position to account for backlash of $\sigma_x = 0.002$ mm, with the photon rate errors coming from the standard deviation of multiple measured rates. Using Eqs. B.11 and B.13, we can calculate the wavelength of the incoming green light at 562 ± 17 nm for the near slit and 585 ± 28 nm for the far slit, both in agreement within one standard deviation to the accepted value of green light at 495-570 nm [8].

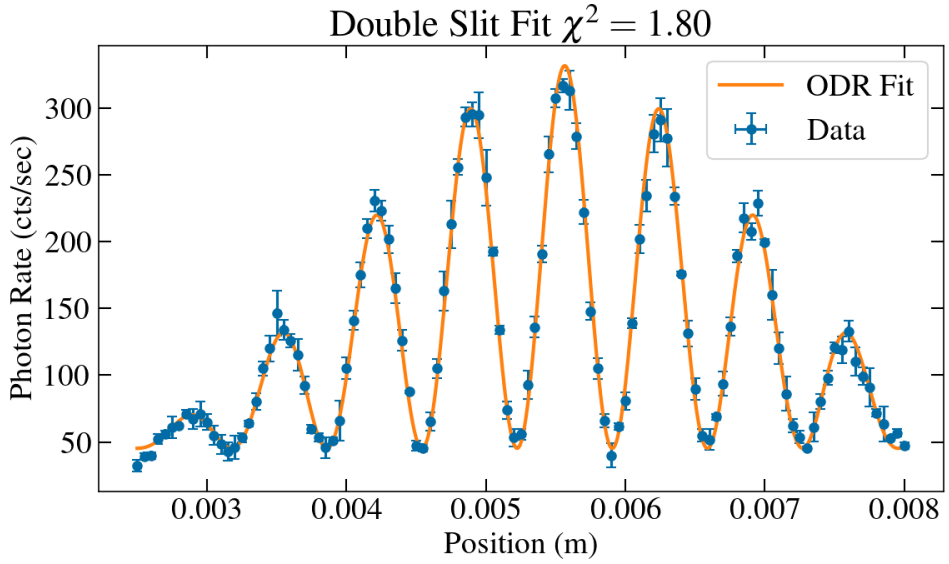

Figure B.4: This figure shows the ODR fit of the double slit (Eq. B.6) for the PMT data. We use the same errors in the micrometer position $\sigma_x = 0.002$ mm. The plotted data points are the average photon rate over multiple readings, with the error bars being the standard deviation of the reading. This fit yields a reduced χ^2 of 1.80, indicating a good fit of our data. Utilizing Eqs. B.12 and B.14, we can extract the wavelength of the light bulb as $\lambda = 561 \pm 4$ nm, which falls within the nominally accepted range of visible green light [8].

From Figures B.3 and B.4, we calculate the wavelength of the light bulb three times: 562 ± 17 nm for the near slit, 585 ± 28 nm for the far slit, and 561 ± 4 nm for the double slit. Using a similar combined result as in Eq. B.10, we complete Young's calculation for our experiment as the wavelength of the light bulb as 561 ± 4 nm. Given that we visibly see the light as green, and given an accepted range for visible green light of 495 to 570 nm [8], our result is within the expected range for general green light. However, given the nominal wavelength in the manual of 541-551 nm [1], our result is 2.5σ away from the anticipated result. This deviation could be attributed to the blackbody distribution of the green filament bulb leaking out more larger wavelength photons or the green filter leaking near-infrared, deep red light, causing an increase in the wavelength calculation.

C Alignment, Shoulder Plots, and Elbow Plots

To align the apparatus, the first thing we ensure is that there is no voltage going through the apparatus, including high voltage, the light source is off, and that the PMT is shuttered properly to protect from damage [2]. We then open the apparatus and remove every slit from the apparatus. This includes the source slit, double slit, slit blocker, and the detector slit. We then turn on the laser and adjust it such that it is accurately pointing towards the detector. Then we place the source slit in the center of the laser beam and diffraction pattern, centered on the detector aperture [2]. Then we place the double slit, also centering it on the diffraction part, and making sure the single slit diffraction pattern is centered on it [2]. Then we place the slit blocker and detector slit. The placement of those are less important because they are on movable stages via micrometers [2]. After doing this, we close the lid and align the detector slit and slit blocker using the micrometers, until we find the maximum voltage, or the center of the double-slit interference pattern [2]. From here we can make the *shoulder plot*. We scan the output voltage of the laser from the photodiode as a function of the slit blocker position. We wish to see "shoulders" on the plot that are as even as possible for best alignment. We can realign multiple times until we are satisfied. The alignment we procured is given in Figure C.1. From the shoulder plot, we can find the optimal regions to place the slit blocker when collecting data for both single slits and the double slit by taking the halfway point of each plateau.

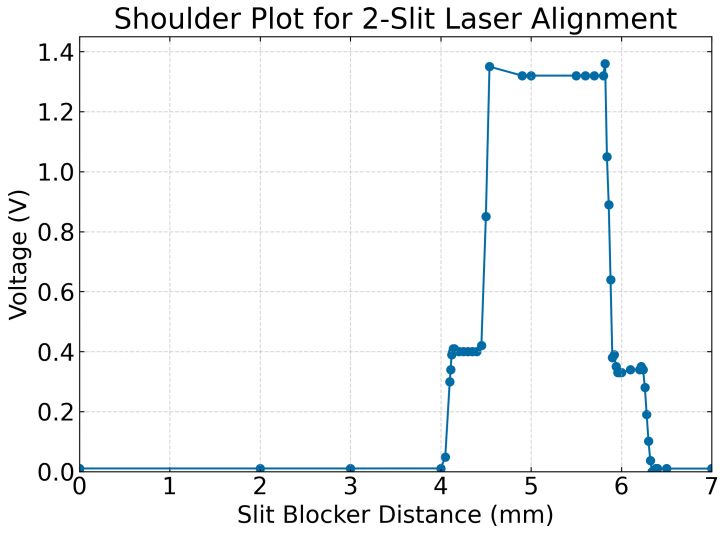

Figure C.1: The shoulder plot for the 2-slit PMT alignment. We see the maximum voltage is at around 1.3V with two shoulders at about 0.4V and 0.37V respectively, which is close to the one-fourth value we expect. From this plot, we can see five distinct regions. In order they are: both slits blocked, the far slit open, both slits open, the near slit open, and then both slits blocked again. In this plot, we don't see perfectly even shoulders, but this slight offset is sufficient for our experiment. From this shoulder plot, we can find the optimal locations to place the slit blocker for each single slit and the double slit, near the center of each plateau. This gives us positions of 4.30 mm for the near slit blocked, 5.20 mm for both slits open, and 6.10 mm for the far slit blocked.

We repeat this process for the PMT, as seen in Figure C.2.

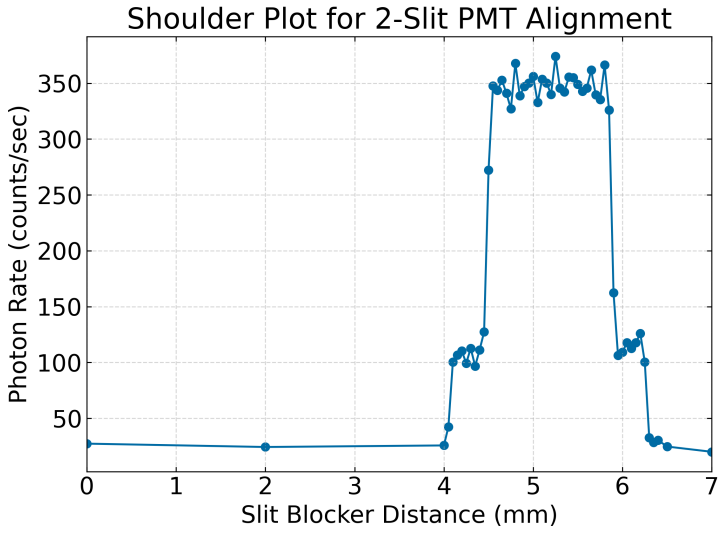

Figure C.2: The shoulder plot for the 2-slit laser alignment. We see the same general shape we expect, as in Figure C.1, with relatively even shoulders. From this plot, we can find the optimal locations to place the slit blocker for our PMT experiment. We get positions of 4.30 mm for the near slit blocked, 5.20 mm for both slits open, and 6.10 mm for the far slit blocked, the same result as in the laser portion of the experiment.

For the PMT experiment, we also produced an elbow plot. The elbow plot shows the dark counts (the number of counts with the PMT shuttered) and the light counts (the number of counts with the PMT not shuttered) as a function of voltage, as seen in Figure C.3. We use this to find the optimal operational voltage of the PMT.

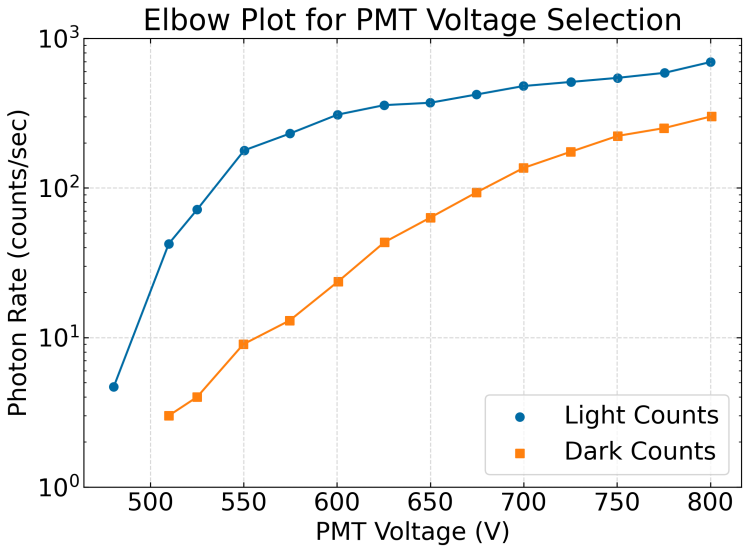

Figure C.3: The elbow plot for the 2-slit PMT alignment. We wish to achieve the best signal contrast possible while operating within a stable range less than 850V [2]. If we set the operating voltage below or on the elbow, our data is more sensitive to noise and fluctuations, but setting the operating voltage too high, the contrast between dark and light counts is not maximized [2]. From this, we set an operating voltage just above the elbow at 600V.

D Single Photon Argument

The time of flight of a photon emitted by the bulb will be given by

$$\Delta t_{\text{flight}} = \frac{D}{c}, \tag{D.1}$$

where D is the distance along the apparatus the photon travels and c is the speed of light. Using our value of $D = 88$ cm [1] and the nominal value of the speed of light, we can calculate this time to be

$$\Delta t_{\text{flight}} \approx 2.77 \text{ ns}.$$

When calculating the total number of photons arriving at the detector per second, we must integrate the count rate over the entire spatial width of the interference pattern rather than simply using the peak intensity. Because a single photon's wave function spreads across the entire diffraction envelope, it has a non-zero probability of landing anywhere along the detector plane. Therefore, the total rate of photons moving through the apparatus must be the sum of the rates across all possible arrival positions.

For our single and double slit data, we can integrate over our counts/sec intensity graphs to get the integer total number of events N via

$$N = \frac{1}{w} \int_{x_{\text{min}}}^{x_{\text{max}}} R(x)\, dx, \tag{D.2}$$

where $R(x)$ is the count rate as a function of the distance x and w is the effective detector slit width of 0.085 mm [1]. Calculating this using our PMT data utilizing a trapezoidal Riemann sum gives us our experimental N values, as seen in Table D.1. From this, we can calculate the *mean separation*, or the average time interval between successive events. This is given by

$$\Delta t_{\text{avg}} \approx \frac{1}{N}. \tag{D.3}$$

These results are also tabulated in Table D.1.

Slit	N	Δt_{avg} (μs)
Near	7201	139
Far	7596	132
Double	11617	86

Table D.1: A table of the slit in question (near, far, or both) and the trapezoidal sum resulting in the total number of counts N that were recorded, which was normalized by the effective detector width of 0.085 mm. From this, we calculate the average time interval between successive events, given by Equation C.3. Integration over the full spatial distribution is required to convert localized point-measurements into a global detection rate that represents the entire photon flux. This aggregate rate ensures the time-of-flight argument accounts for all photons entering the apparatus, rather than just the small fraction captured at the interference peak. We compare the worst case for the average time between events (the shortest time, or 86 μs) to the calculated time of flight using Equation C.1. Applying Poisson statistics, we find that the probability that there is more than one photon in the apparatus is 3.24×10^{-7}, meaning we are recording single photon events.

To prove singular photon events, we will use the *worst* result for Δt_{avg}, which for us is the shortest time, or 86 μs. We also need to take into account that the PMT only receives about 4% of all photon events [1]. This means that our Δt will be 0.04×86 μs or 3.44 μs. From this, we can calculate the mean number of photons μ present in the apparatus during a single time of flight window:

$$\mu = \frac{\Delta t_{\text{flight}}}{\Delta t_{\text{avg}}} \approx 8.05 \times 10^{-4}. \tag{D.4}$$

We will now argue the probability of there being more than one photon in the detector at a time, which relies on the assumption that each photon is given off randomly [2]. We utilize Poisson statistics:

$$P(k) = \frac{e^{-\mu}\mu^k}{k!}, \tag{D.5}$$

for some event k. To calculate the probability that there is more than one photon in the apparatus, we can leverage the fact that the total probability for any number of photons in the apparatus is 1. If k is the number of photons, this means that

$$P(k > 1) = 1 - P(0) - P(1) = 1 - e^{-\mu} - e^{-\mu}\mu. \tag{D.6}$$

Plugging in our value for μ, this gives us

$$P(k > 1) \approx 3.24 \times 10^{-7}. \tag{D.7}$$

This shows that a great majority of the time, the apparatus is either empty $k = 0$ or has only a singular photon $k = 1$. We also show that the probability of a single photon is not completely negligible,

$$P(k = 1) = \mu e^{-\mu} \approx 9 \times 10^{-4}. \tag{D.8}$$

Hence, about 99.9% of the time, the apparatus is empty, with the remaining 0.1% of the time there

is only a singular photon, whereas there is less than 0.00003% chance that there is more than one photon in the box. This provides strong statistical evidence of single photon events [2].